Thermodynamic Properties of Multialkane Synthetic and Real Petroleum Mixtures

Anne-Julie Briard, Mohammed Bouroukba, D. Petitjean, and Michel Dirand*

Laboratoire de Thermodynamique des Milieux Polyphasés, EA no. 3099, Ecole Nationale Supérieure des Industries Chimiques, Institut National Polytechnique de Lorraine, 1, rue Grandville, BP 451, F-54001 Nancy Cedex, France

Measurements of enthalpy increments from the temperature of the ordered phases of low temperatures at 293.4 K up to the liquid phase above the melting point were carried out by differential scanning calorimetry using discontinuous mode temperature programming on 18 multiparaffinic mixtures, prepared by melting pure alkanes, and 4 commercial petroleum waxes. Temperatures and enthalpies of the solid/solid transitions and melting were determined, as well as the total enthalpy variations from the order/disorder transition onset temperature up to the melting end temperature and the heat capacity variations in the ordered solid solution and the liquid phase, as a function of temperature. The comparison of the experimental results with the values, calculated for equivalent ideal mixtures from the thermodynamic data of pure *n*-alkanes, allows us to highlight a deviation in relation to the ideality in the solid state for all of these mixtures: the ordered solid phase reveals a significant gap in relation to ideality, whereas the liquid mixtures show athermal behavior. The composition characteristic parameters of the mixtures (shape of the *n*-alkane mole fraction distribution, number of *n*-alkanes, and percentage of the other nonlinear hydrocarbons in the petroleum mixtures) are closely related to the degree of internal disorder in the solid solutions and thus to the deviation in relation to the ideality in the solid state.

Introduction

The formation of solid deposits during the exploitation, transportation, and refining process of paraffinic crude oils is a major issue for the petroleum industry: the removal of the undesirable solids increases production costs. A better understanding of the complex *n*-alkane (hereafter denoted by C_n) mixtures and the development of thermodynamic models enable us to predict their onset crystallization point, which will make it possible to adjust process operating parameters and reduce costs. The modeling requires thermodynamic data (phase-transformation temperatures and enthalpies, heat capacities) of all pure components and pseudoconstituents occurring in the solid/liquid equilibria.

A previous paper[1] proposed simple predictive relationships concerning the variations of the pure C_n thermodynamic properties as functions of the *n* carbon atom number of the C_n chain by combining new calorimetric experimental results[2] with a general review of literature data.[3,4]

In this article, the thermodynamic properties of complex multi-C_n mixtures are obtained by differential scanning calorimetry to determine their thermodynamic characteristics in relation to the ideality in the solid phase and the liquid phase, also required for their modeling.

Further Details

The term "synthetic mixtures", previously quoted in the literature,[4−17] is applied to the multi-C_n mixtures obtained in the laboratory from 2, 3, 4...*N* pure C_n's by the melting process and is used in relation to the term multi-C_n "real mixtures" from industrial or commercial origin.

* Corresponding author. E-mail: mdirand@ensic.inpl-nancy.fr. Tel: 33-(0)3-83-17-50-07. Fax: 33-(0)3-83-17-50-76.

Structural analyses carried out recently by X-ray diffraction on synthetic and real multi-C_n complex mixtures highlighted the influence of specific parameters of the sample composition[4−17] on the final crystalline state, as follows:

(i) the width (number of C_n's, *N*) of the continuous distribution of x_n mole fractions of consecutive C_n's, determined by comparing 16 synthetic mixtures with x_n distributions of the exponential decreasing type[4] ($x_{n+1} = 0.858x_n$; Figure 1a) and *N* numbers of consecutive C_n's from $2 \leq N \leq 21$;

(ii) the shape of x_n distributions determined by comparing two C_{22}−C_{36} synthetic samples from C_{22} up to C_{36} ($N = 15$) with two different[4] x_n distributions—one of normal logarithmic (or Gaussian) type and the other of exponential decreasing type (Figure 1);

(iii) the standard deviation and the *n* real mean carbon atom number of the x_n distribution determined by comparing two C_{22}−C_{36} synthetic mixtures with x_n distributions of the normal logarithmic type, whose x_n compositions of C_n's are different;

(iv) the percentage of nonlinear hydrocarbons determined by comparing real and synthetic mixtures whose x_n distributions of the normal logarithmic type are identical.

The aim of our experimental calorimetric studies is to complete the previous structural analyses[4−11] and to determine the influence of the composition parameters on the thermodynamic properties.

Synthetic Mixtures with C_n Mole Fraction Distributions of the Exponential Decreasing Type

Sample Preparation. The industrial and commercial multi-C_n samples that have been studied in the literature[5−7,9,10] show a continuous x_n distribution of the normal

10.1021/je0302405 CCC: $27.50
Published on Web 08/12/2004

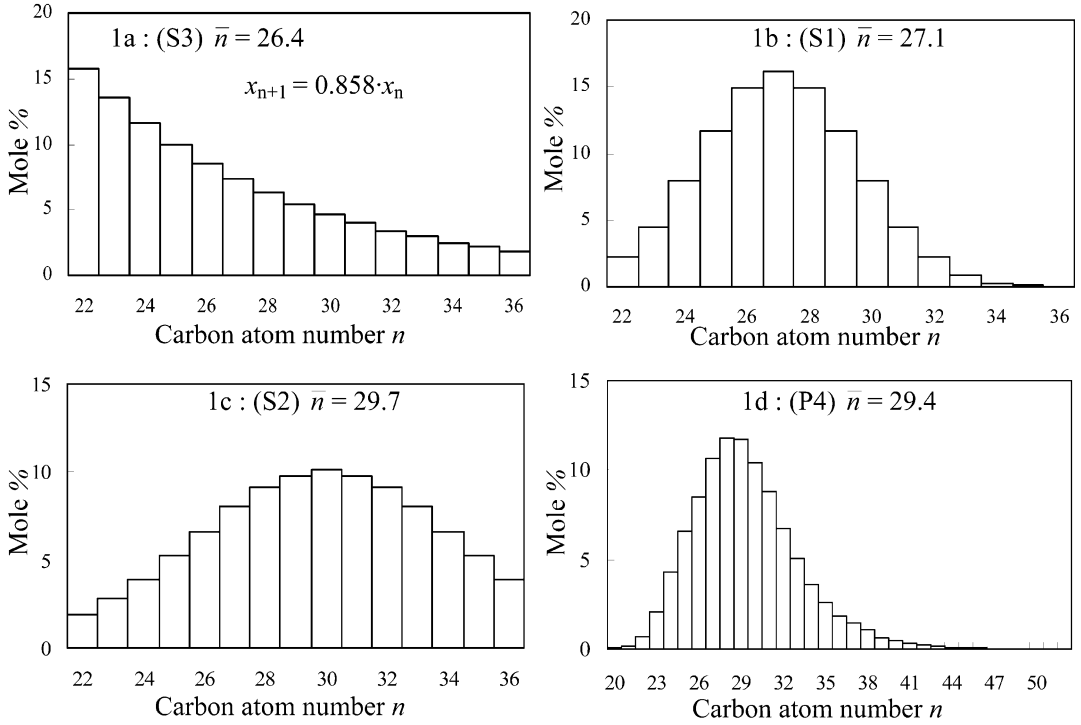

Figure 1. Shapes of the x_n distributions of S1, S2, and S3 mixtures containing 15 identical C_n's and a P4 real mixture: (a) distribution of exponential decreasing type (S3); (b−d) distributiuon of the normal logarithmic or Gaussian type (S1, S2, P4).

Table 1. Group 1, 2, and 3 Mixtures with x_n Distributions of the Exponential Decreasing Type[a]

			first solid solution			second solid solution			third solid solution		
mixtures	N	$\bar{n}$	c/Å	$\bar{n}_c$	structure	c/Å	$\bar{n}_c$	structure	c/Å	$\bar{n}_c$	structure
$C_{24}-C_{25}$	2	24.5	66.2	24.2	$\beta' + \beta''$						
$C_{24}-C_{26}$	3	24.9	66.8	24.8	β''						
$C_{22}-C_{25}$	4	23.3	62.7	23.2	β'						
$C_{21}-C_{25}$	5	22.7	61.4	22.6	β'						
$C_{22}-C_{27}$	6	24.1	64.4	23.8	β'						
$C_{22}-C_{29}$	8	24.7	66.7	24.7	β'						
$C_{22}-C_{30}$	9	25.0	67.8	25.2	β'						
$C_{22}-C_{33}$	12	25.8	67.3	25.0	β'	71.2	26.5	β'			
$C_{22}-C_{35}$	14	26.2	67.3	25.0	β'	75.1	28.0	β'			
$C_{22}-C_{36}$ [b]	15	26.4	67.5	25.0	β'	82.1	30.8	β'			
$C_{21}-C_{36}$	16	25.5	66.0	24.4	β'	83.6	31.3	β'			
$C_{20}-C_{36}$	17	24.7	63.3	23.4	$\beta' + \beta$-RI	84.1	31.6	β'	65.9	24.4	β'
$C_{19}-C_{36}$	18	23.8	61.9	22.8	β-RI	80.0	30.0	β'	72.9	27.2	β'
$C_{18}-C_{36}$	19	23.0	59.8	22.0	β-RI	83.7	31.4	β'	76.7	28.6	β'
$C_{17}-C_{36}$	20	22.1	58.9	21.7	β-RI	86.1	32.4	β'	73.8	27.5	β'
$C_{16}-C_{36}$	21	21.2	56.8	20.8	β-RI + α-RII	82.5	30.9	β'	74.6	27.8	β'

[a] Evolution of the crystalline solid phase number, long c parameter, $\bar{n}_c$ (mean carbon atom number), and crystalline structure as a function of the N number of C_n's in each sample, with $\bar{n}$ corresponding to the mean carbon atom number of the mixtures. [b] Mixture corresponding to the S3 sample.

logarithmic type (Figure 1d). Here, 16 samples were composed of consecutive C_n's whose x_n mole fractions decrease regularly according to the recurrence relationship $x_{n+1} = \alpha x_n$. The coefficient α was fixed at 0.858 because this value corresponded to the average compositions observed in crude oils (Figure 1a). The mixtures were prepared by mass from solid pure C_n's, followed by melting and thoroughly mixing. The homogeneous paraffinic liquid solution was allowed to cool to ambient temperature. All of the pure C_n's were purchased from Fluka; their purity was ≥98%, as determined by our gas chromatography analyses. The multi-C_n mixtures were split into three characteristic groups (Table 1):

(i) group 1: four mixtures composed of a consecutive C_n number, N, as follows: $2 \le N \le 5$ ($C_{24}-C_{25}$, $C_{24}-C_{26}$, $C_{22}-C_{25}$, and $C_{21}-C_{25}$);

(ii) group 2: six mixtures with a middle width of x_n distributions ($6 \le N \le 15$) going from $C_{22}-C_{27}$ to $C_{22}-C_{36}$; the lightest C_n is always C_{22}, and these distributions differentiate themselves by the successive addition of heavier C_n's from C_{27} to C_{36}.

(iii) group 3: six mixtures with larger x_n distributions ($16 \le N \le 21$) going from $C_{21}-C_{36}$ to $C_{16}-C_{36}$: the heaviest C_n is always C_{36}, and these distributions differentiate themselves by the successive addition of lighter C_n's from C_{22} up to C_{16}.

X-ray Diffraction Studies. All of these solid samples were analyzed by X-ray diffraction at ambient temperature (T = 294.15 K) according to two methods:

(i) A Guinier de Wolff Nonius camera was used to characterize the structure of the solid phases. This method provides a good separation of the Bragg reflections, especially in the 21−22° region of Bragg angles, where the symmetry of the structure can be identified. These experiments were carried out on powder samples using λKα copper radiation (Figure 2). The spacing between two

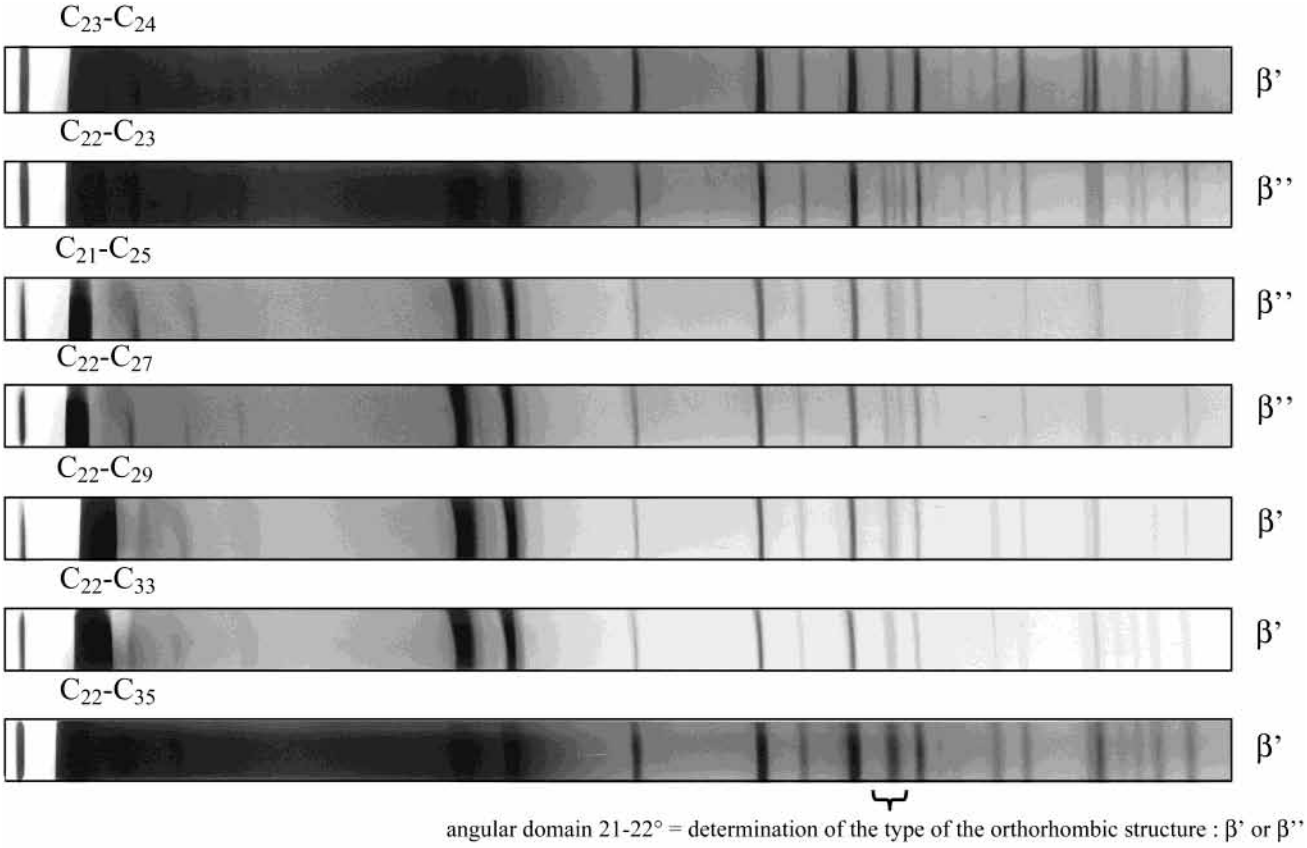

Figure 2. Structural identifications of multi-C_n mixtures with distributions of the exponential decreasing type by comparison with the powder X-ray diffraction patterns carried out on binary mixtures (C_{23} + C_{24}) and (C_{22} + C_{23}), whose β' and β'' intermediate-phase orthorhombic structures are known.

reflections was measured with an accuracy of 0.25 mm for distances ranging from 10.5 to 125 mm. Corrections were made employing spectroscopic pure gold as a standard. The exposure time of the films was fixed at 24 h for all experiments.

(ii) A counter diffractometer (λKα copper radiation) was used to bring out the number of solid solutions and their lattice parameters, especially the *c*-axis crystalline parameter along the carbon chains. The Bragg angle values were measured with an accuracy of 0.05°. The samples were prepared by slow cooling on a water surface of the melted C_n mixtures. This mode of sample preparation does not change the structural state of multi-C_n mixtures and allows us to increase the intensity of the (00*l*) diffraction lines by preferential crystallographic orientations, the carbon chains being perpendicular to the water surface. This experimental method allows to accurately determine

−the number of crystalline solid phases in the sample from the number of series of (00*l*) harmonic diffraction peaks and

−the $\bar{n}_c$ mean number of carbon atoms per molecule of each phase, determined from the experimental values of their *c* crystalline parameter.

Indeed, $\bar{n}_c$ is calculated according to the relationship, established by Chevallier et al.[12] from the structural data of literature, concerning (*Pbcm*) orthorhombic pure odd-numbered C_n's ($n \leq 41$,)[4,13] as follows:

$$c/\text{Å} = 2.5448\bar{n}_c + 3.7504 \qquad \text{with} \qquad c/\text{Å} = 2d_{(002)}$$

$$\bar{n}_c = \frac{c - 3.7504}{2.5448}$$

$d_{(002)}$/Å is equal to the thickness of the molecular layer in the orthorhombic structure of pure odd-numbered C_n's and molecular alloys. This thickness is equal to the length of the "average molecule" in the multi-C_n phase.

Note that the real average $\bar{n}$ of carbon atoms per molecule of mixture is calculated by the following relationship:

$$\bar{n} = \sum_{n_{\min}}^{n_{\max}} x_n n$$

with $n_{\max}$ and $n_{\min}$, respectively, being the number of carbon atoms of the longest and the shortest C_n's of the distribution. x_n is the mole fraction, and *n* is the number of carbon atoms of each C_n.

The characteristic structural parameters of these single-phase or polyphase samples, the number of crystallized solid solutions at ambient temperature, the crystalline *c* parameter and the $\bar{n}_c$ mean number of carbon atoms of the solid phases, the crystallographic structure, and the $\bar{n}$ real mean number of carbon atoms of the distribution are provided in Table 1. All of these structural data are necessary to understand the differences in the thermodynamic properties from one mixture to another.

(i) The mixtures of groups 1 and 2 with $N \leq 11$ form a single solid phase whose orthorhombic structure is isostructural to the β' or β'' ordered intermediate phase of binary and ternary C_n alloys.[14−16] A single periodicity of the molecular layer stacking along the long crystallographic *c* axis is observed; it corresponds to the mean chain length of a hypothetical orthorhombic odd-numbered C_n with a $\bar{n}_c$ number of carbon atoms equal to the $\bar{n}$ real mean number of carbon atoms of multi-C_n mixtures with an

Table 2. Experimental Thermodynamic Properties of Group 1, 2, and 3 Mixtures[a]

					melting			order/disorder		total	
mixtures	$\bar{n}$	$\bar{M}$/ g·mol^{-1}	N of C_n's	number of solid solutions	ΔT_{fus}(exptl) /K	$\Delta_{fus}H$(exptl) /kJ·mol^{-1}	$\Delta_{fus}h$(exptl) /J·g^{-1}	ΔT_{o-d}(exptl) /K	ΔH_{o-d}(exptl) /kJ·mol^{-1}	$\Delta H^{T_{fus}}_{T_{o-d}}$ /kJ·mol^{-1}	$\Delta h^{T_{fus}}_{T_{o-d}}$ /J·g^{-1}
$C_{24}-C_{25}$	24.5	344.7	2	2	323.9−325.0	56.0	162.4	313.6−316.0	22.1	89.2	258.9
$C_{24}-C_{26}$	24.9	350.8	3	1	324.9−326.0	54.2	154.6	312.6−315.1	18.7	86.1	245.4
$C_{22}-C_{25}$	23.3	328.6	4	1	319.4−320.9	48.9	149.0	302.2−305.0	12.4	84.5	257.3
$C_{21}-C_{25}$	22.7	320.0	5	1	317.5−319.0	47.1	147.3	297.2−300.6	10.3	77.5	242.1
$C_{22}-C_{27}$	24.1	339.1	6	1	321.3−323.0	52.2	155.0	302.4−306.1	11.1	83.6	246.5
$C_{22}-C_{29}$	24.7	348.3	8	1	322.7−325.3	53.7	154.2	302.8−308.0	12.9	85.3	244.8
$C_{22}-C_{30}$	25.0	352.4	9	1	322.4−325.8	52.5	148.8	302.4−307.1	12.4	84.4	239.6
$C_{22}-C_{33}$	25.8	363.1	12	2	322.4−326.9	52.6	143.8	301.8−306.0	9.7	84.5	232.8
$C_{22}-C_{35}$	26.2	368.9	14	2	322.4−328.0	51.6	139.8	301.3−306.7	13.3	85.9	233.0
$C_{22}-C_{36}$	26.4	371.4	15	2	322.5−329.8	52.1	140.4	302.2−306.0	8.3	88.1	237.3
$C_{21}-C_{36}$	25.5	359.7	16	2	319.9−328.7	47.8	132.8	297.0−300.9	7.6	83.5	232.0
$C_{20}-C_{36}$	24.7	347.8	17	2	317.1−327.6	47.2	135.8	*b*	*b*		
$C_{19}-C_{36}$	23.8	335.8	18	3	312.9−326.5	43.7	130.2	*b*	*b*		
$C_{18}-C_{36}$	22.9	323.5	19	3	306.7−324.6	44.2	136.6	*b*	*b*		
$C_{17}-C_{36}$	22.1	303.1	20	3	304.6−325.8	42.0	138.6	*b*	*b*		
$C_{16}-C_{36}$	21.2	298.5	21	3	301.4−325.7	42.4	142.0	*b*	*b*		

[a] $\Delta T_{fus}(\pm 0.5)$/K, temperature range of melting; $\Delta_{fus}H$/kJ·mol^{-1} and J·g^{-1} (% diff = 3%), enthalpy of melting; $\Delta T_{o-d}(\pm 0.5)$/K, temperature range of order/disorder transition; ΔH_{o-d}/kJ·mol^{-1} and J·g^{-1} (% diff = 3%), enthalpy of order/disorder transition; $\Delta H^{T_{fus}}_{T_{o-d}}$/kJ·mol^{-1} and J·g^{-1} (% diff = 3%), enthalpy variation from T_{o-d} to $T_{fus(end)}$. [b] Not measured.

excess value close to one carbon atom[5,6] ($\bar{n}_c \approx \bar{n} + 1$). Thus, all C_n's combine into a single molecular layer: the longer molecules bend to insert themselves between the stacking planes and associate with shorter molecules to obtain a single solid solution with a dense structure.

(ii) The other samples of group 2 ($12 \leq N \leq 15$) crystallize into two solid solutions with the same orthorhombic structure β' but with different $\bar{n}_c$ mean numbers of carbon atom. The successive addition of heavier C_n's to the distribution induces the instability of the multi-C_n solid solution and the emergence of a second solid phase, richer in heavy C_n's; the increase in the chain lengths' disparity requires a second molecular layer to combine all C_n's into dense and stable orthorhombic structures. The heavy C_n's that are added insert themselves into the structure whose stacking periodicity is compatible with their own chain length in order to minimize the molecular length gaps; they crystallize into the new heavy phase, whose $\bar{n}_c$ average chain length gradually increases. The lighter phase, with a lower layer thickness, cannot accommodate these new heavy C_n's and thus keeps an unchanged $\bar{n}_c$ average composition.

(iii) For the mixtures of group 3, the broading of the C_n distribution ($16 \leq N \leq 21$) toward lighter C_n's involves the emergence of a third solid solution with a middle value of the $\bar{n}_c$ mean number of carbon atoms. This new solid phase is generated by the miscibility gap in the solid state of the light phase whose structure becomes unstable by the progressive intercalation of new light C_n's and an increase in the chain lengths' disparity. The lighter C_n's that are added crystallize mainly into the lighter phase; the $\bar{n}_c$ mean number of carbon atom of this latter phase gradually decreases, whereas the average $\bar{n}_c$ number of carbon atoms of the two other phases remains invariant.

The main observation is that the number of crystallized solid solutions increases with the N number of x_n distribution C_n's of mixtures.

Principle of Measurement and Operating Conditions. The detailed principle of measurements and the description of the experimental method are defined in the literature,[2,18−20] with further details of the estimations of uncertainties in accuracy and reproductibility. The measurements of the enthalpy increments ($H^T_{T_o}$/kJ·mol^{-1}; T_o = 293.4 K) were deduced from differential thermal analyses, performed with a differential scanning calorimeter of the Tian−Calvet type[21] (SETARAM DSC 111) using a discontinuous mode of temperature programming.[2,18−20] The repeatability and the accuracy of enthalpy and temperature measurements have been determined by using pure *n*-alkanes C_{18} and C_{26}.[2,18−20] The experimental enthalpy values are in good agreement with the literature results,[22,23] and this agreement justifies the experimental method used (percent difference < 1.5%); the accuracy of the temperature measurements is equal to ±0.5 K.

Table 3. Experimental Specific Enthalpies of Phase Transformations of Group 3 Mixtures Determined by the DSC Continuous Method

mixtures	Δh_{o-d}/J·g^{-1}	Δh_{d-d}/J·g^{-1}	$\Delta_{fus}h$/J·g^{-1}	$\Delta h^{T_{fus}}_{T_{o-d}}$/J·g^{-1}
$C_{22}-C_{36}$	22.6	3.1	145.0	241.2
$C_{21}-C_{36}$	22.1	3.3	135.9	237.5
$C_{20}-C_{36}$	17.1	3.3	138.1	235.8
$C_{19}-C_{36}$	18.0	3.2	134.3	231.2
$C_{18}-C_{36}$		2.9	140.1	
$C_{17}-C_{36}$		3.0	142.9	
$C_{16}-C_{36}$		2.6	141.3	

The samples richest in light C_n's of group 3 (from $C_{20}-C_{36}$ to $C_{16}-C_{36}$) are in equilibrium (liquid + solids) at 293.15 K, and differential thermal analyses (DTA) were performed with another differential scanning calorimeter of the Tian−Calvet type[21] (SETARAM DSC III) using a continuous mode of temperature programming with cooling or heating by the Peltier effect: the mixtures were heated from 263.15 K to 343.15 K at a rate of 0.5 K·min^{-1}. The detailed principle of this device, which is very sensitive, and the description of the experimental method are defined in the literature.[24]

Results and Discussion. The experimental order/disorder transition and melting onset and ending temperatures, the (ΔH/kJ·mol^{-1} and Δh/J·g^{-1}) phase transformation enthalpies, and the ($\Delta H^{T_{fus}}_{T_{o-d}}$/kJ·mol^{-1} and $\Delta h^{T_{fus}}_{T_{o-d}}$/J·g^{-1}) enthalpy variations from the T_{o-d} order/disorder transition onset temperature up to the liquid are reported in Tables 2 and 3.

(a) Enthalpy Increment Curves. The experimental enthalpies ($H^T_{T_o}$/kJ·mol^{-1}; T_o = 293.4 K) variations of 16

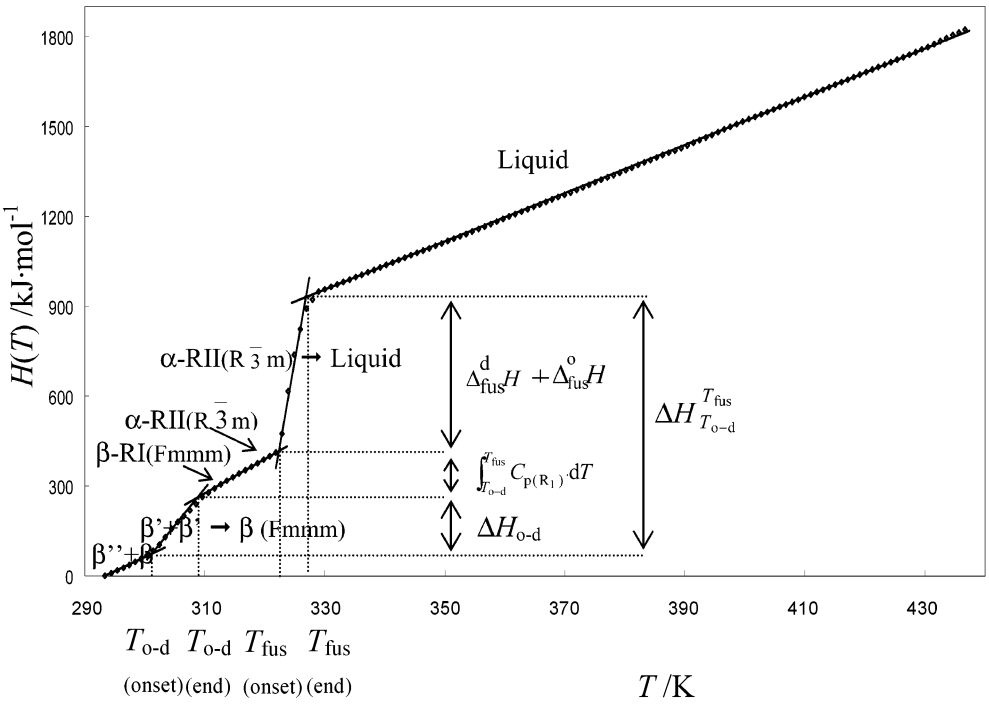

Figure 3. Enthalpy curve ($H^{T}_{T_o}$/kJ·mol^{-1}; T_o = 293.4 K) of the $C_{22}-C_{35}$ multi-C_n mixture of group 2 from the two-phase ($\beta' + \beta''$) ordered solid state up to the liquid phase.

multi-C_n samples with respect to the temperature are listed in Supporting Information. Figure 3 shows the enthalpy increment curve as a function of increasing temperature, obtained for the two-phase sample $C_{22}-C_{35}$. With increasing temperature, the solid solution of single-phase systems or only the lighter phase of polyphase mixtures undergoes solid/solid transitions identical to those of the orthorhombic odd-numbered pure C_n[1−7,12,14,16,17] (Figure 3):

$$\beta' \text{ or } \beta'' \xrightarrow{T_{o-d}} \beta(Fmmm) \Rightarrow \beta\text{-RI}(Fmmm) \xrightarrow{T_{d-d}} \alpha\text{-RII}(R\bar{3}m) \xrightarrow{T_{fus}} \text{liquid}$$

where → denotes first-order transitions and ⇒ denotes higher-order transitions.

In polyphase systems, the β' middle or heavier phases do not undergo any solid/solid transition up to the liquid phase, and the $\Delta H^{T_{fus}}_{T_{o-d}}$ enthalpy variations can be decomposed into the following terms:

(i) single-phase sample:

$$\Delta H^{T_{fus}}_{T_{o-d}} = \Delta H_{o-d} + \int_{T_{o-d}}^{T_{fus}} C_{p(R1)}\,dT \quad (\text{or} + \int_{T_{o-d}}^{T_{d-d}} C_{p(R1)}\,dT + \Delta H_{d-d} + \int_{T_{d-d}}^{T_{fus}} C_{p(R2)}\,dT)^* + \Delta^{d}_{fus}H$$

with ΔH_{o-d} and ΔH_{d-d}, enthalpies of order/disorder and disorder/disorder solid/solid transitions; T_{o-d} and T_{d-d}, onset temperatures of order/disorder and disorder/disorder solid/solid transitions; $\Delta^{d}_{fus}H$, enthalpy of melting of the disordered rotator phase (R_1 or R_2), stable below the melting onset temperature; T_{fus}, the melting temperature;

$$\int_{T_{o-d}}^{T_{fus}} C_{p(R1)}\,dT, \int_{T_{o-d}}^{T_{d-d}} C_{p(R1)}\,dT, \text{ and } \int_{T_{d-d}}^{T_{fus}} C_{p(R2)}\,dT,$$

the enthalpy consumption in the temperature domains of rotator phases; and $C_{p(R1)}$ and $C_{p(R2)}$, the heat capacities of the β-RI($Fmmm$) and α-RII($R\bar{3}m$) disordered rotator phases[1−7,17].

(ii) polyphase sample:

$$\Delta H^{T_{fus}}_{T_{o-d}} = \Delta H_{o-d} + \int_{T_{o-d}}^{T_{fus}} C_{p(R1)}\,dT \quad (\text{or} + \int_{T_{o-d}}^{T_{d-d}} C_{p(R1)}\,dT + \Delta H_{d-d} + \int_{T_{d-d}}^{T_{fus}} C_{p(R2)}\,dT)^* + \Delta^{d}_{fus}H + z(\Delta^{o}_{fus}H + \int_{T_{o-d}}^{T_{fus}} C_{p(\beta')}\,dT)$$

with z, the number of β' solid solutions, stable up to the melting point;

$\Delta^{o}_{fus}H$, the enthalpy of melting of the β' ordered orthorhombic structure;

$C_{p(\beta')}$, the heat capacity of the β' ordered orthorhombic structure; and

$$^*(\int_{T_{o-d}}^{T_{d-d}} C_{p(R1)}\,dT + \Delta H_{d-d} + \int_{T_{d-d}}^{T_{fus}} C_{p(R2)}\,dT)$$

if the disorder/disorder solid/solid transition is observed in the sample.

(b) Phase-Transformation Temperatures. Figure 4 represents the variations in the onset temperatures of the order/disorder transition and melting in relation to the $\bar{n}$ real average number of carbon atoms of the mixtures and the $\bar{T}_{fus}$ average melting temperatures, calculated by a linear combination of the $T_{fus\ i}$ melting temperatures of pure C_n's ($\bar{T}_{fus} = \Sigma_{i=1}^{N} x_i\ T_{fus\ i}$).

These variations in the experimental transformation temperatures point out three particular behaviors linked to the x_n distribution of mixtures, particularly to the value of the $\bar{n}_c$ mean number of carbon atoms of the solid solution that undergoes solid/solid transitions:

(i) For the single-phase mixtures of groups 1 and 2 ($N \leq 11$), the experimental melting points increase with respect

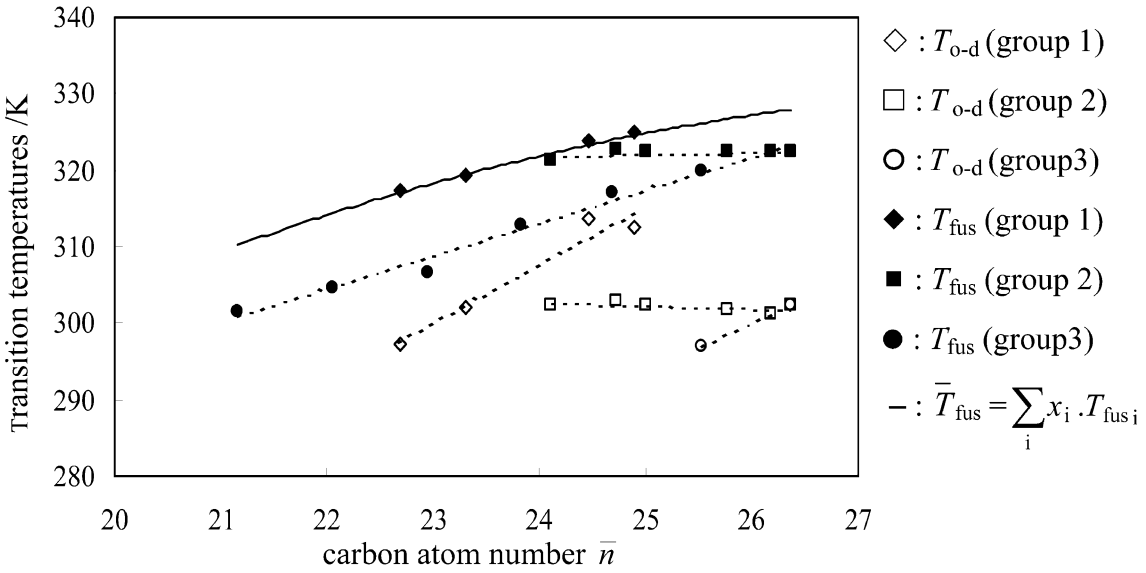

Figure 4. Transformation onset temperatures of mixtures of groups 1−3 compared to the variations in the ($\bar{T}_{fus} = \Sigma_{i=1}^{N} x_i T_{fus\ i}$) average melting temperatures versus the $\bar{n}$ real mean number of carbon atoms of the mixtures.

to $\bar{n}$, the average number carbon atoms of mixtures, and are brought into alignment with the $\bar{T}_{fus}$ average values calculated (Figure 4). Below the fusion temperature, these mixtures show a disordered rotator state that is close to ideality according to the literature.[25−28]

(ii) For the two-phase mixtures of group 2, the onset temperatures of the order/disorder transition and melting are lower than those of group 1 samples and remain invariant because the $\bar{n}_c$'s, mean numbers of carbon atoms, of the lightest solid solution of two-phase mixtures are almost equal and close to 25 (Table 1). These observations confirm the structural results of the X-ray diffraction studies: the addition of heavy C_n to the distribution affects only the heaviest phase, the average composition of the light solid solution remaining unchanged.

(iii) For the seven mixtures of group 3, the onset temperatures of the order/disorder transition and the melting decrease (Figure 4). Indeed, according to the structural observations by X-ray diffraction, the $\bar{n}_c$ mean number of carbon atoms of the lightest phase decreases in relation to the successive addition of lighter C_n's (Table 1).

Note that the $\bar{n}$ real average number of carbon atoms of polyphase mixtures is not the only parameter to take into account in the melting-point estimation. It is necessary to know the $\bar{n}_c$ average composition of each phase in the polyphase systems.

The ΔT gap between the temperatures of the onset and end of fusion also varies in relation to the width of the x_n distribution. Figure 5 represents the ΔT ($\Delta T = T_{fus(onset)} - T_{fus(end)}$) variations as a function of the N number of C_n's of the x_n distribution. Three behaviors can be distinguished:

(i) Single-phase systems: ΔT increases linearly with a weak slope (Figure 5).

(ii) Two-phase systems of group 2: ΔT also increases linearly with a higher slope (Figure 5); $T_{fus\ (onset)}$, depending on the lightest solid phase, whose $\bar{n}_c$ is constant, is invariant (Figure 4), whereas $T_{fus(end)}$ increases as a function of the progressive enrichment of a heavier phase in heavy C_n's.

(iii) Three-phase systems of group 3: ΔT varies exponentially (Figure 5) because $T_{fus(onset)}$ strongly decreases with the important enrichment of low-molecular-mass C_n's in the lightest phase but $T_{fus(end)}$ is constant, the average composition of the heaviest phase remaining unchanged.

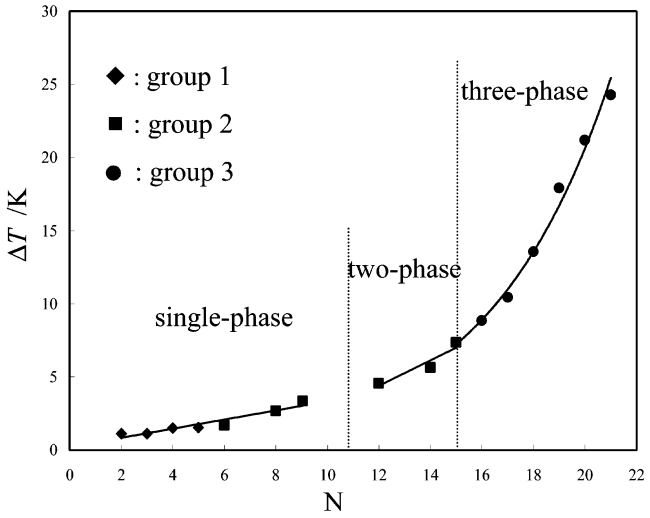

Figure 5. Variations of the ΔT gap ($\Delta T = T_{fus(onset)} - T_{fus(end)}$) as a function of the N number of C_n's in the samples.

(c) Phase-Transformation Enthalpies. The variations in the Δh_{o-d} order/disorder transition specific enthalpies, the $\Delta_{fus}h$ melting specific enthalpy, and the $\Delta h_{T_{o-d}}^{T_{fus}}$ total specific enthalpy are represented in Figure 6 as functions of the $\bar{n}$ real average number of carbon atom of the mixtures. The experimental phase-transition specific enthalpies are scattered around a mean value, independent of the N number of mixture C_n's (Tables 2 and 3): Δh_{o-d}/J·g^{-1} = 36.3 ± 1.1; $\Delta_{fus}h$/J·g^{-1} = 144.5 ± 4.3; $\Delta h_{T_{o-d}}^{T_{fus}}$/J·g^{-1} = 242.3 ± 7.3

The experimental measurements, determined by DSC and DTA (Tables 2 and 3), are compared with the values calculated from the thermodynamic data[1−4,17] of pure C_n's for equivalent ideal mixtures: ($\Delta\bar{h} = \Sigma_{i=1}^{N} x_i \Delta h_i$; Δh_{o-d}/J·g^{-1} = 72; $\Delta_{fus}h$/J·g^{-1}= 165; $\Delta h_{T_{o-d}}^{T_{fus}}$/J·g^{-1} = 269) (Figure 6). The difference between the experimental and calculated values allows us to estimate the deviation in relation to the ideality of mixtures. Figure 6 shows that this difference is always positive.

Indeed, C_n molecules tend to move away in the paraffinic system to minimize the energies of interaction; the association of molecules of different lengths to form a stable molecular layer in a single solid phase requires a supple-

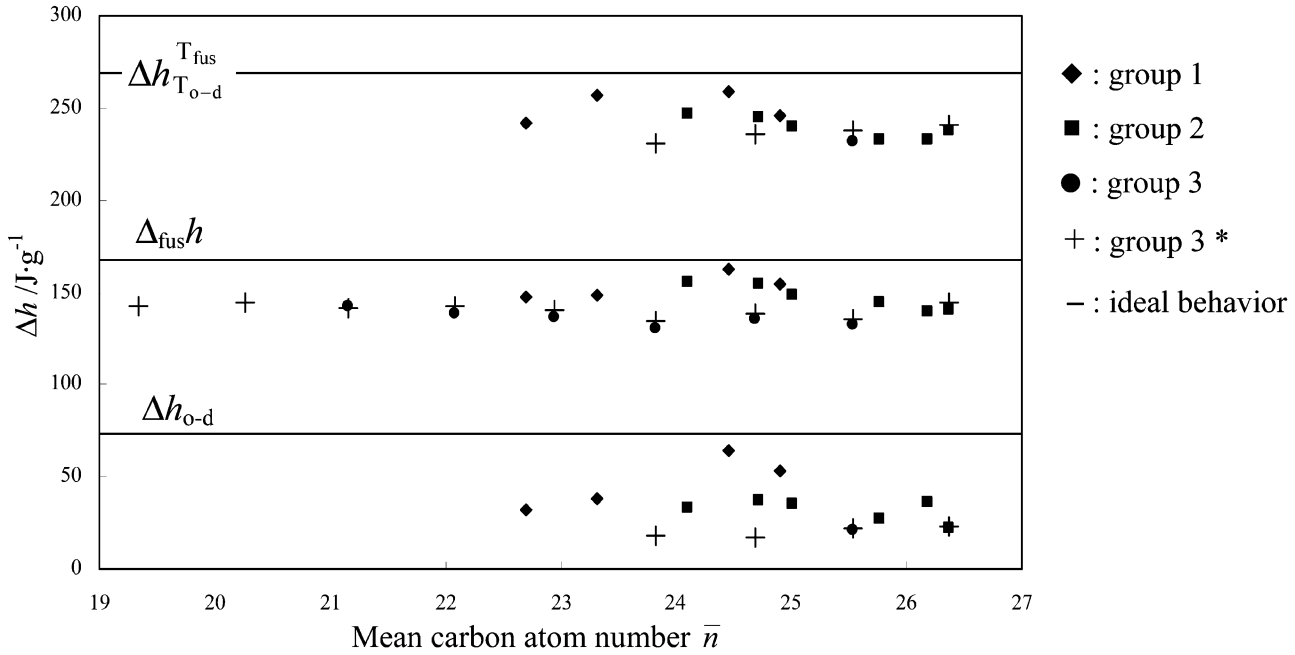

Figure 6. Comparison between the experimental specific enthalpies of phase transformations of the mixtures of groups 1−3 versus the $\bar{n}$ mean number of carbon atoms in the samples and the values calculated for the equivalent ideal mixtures[1]: $\Delta h^{T_{fus}}_{T_{o-d}}$/J·g^{-1} = 269; $\Delta^{d}_{fus}h$/J·g^{-1}= 165; Δh_{o-d}/J·g^{-1} = 72; * experimental values (+) determined by the DSC continuous method.

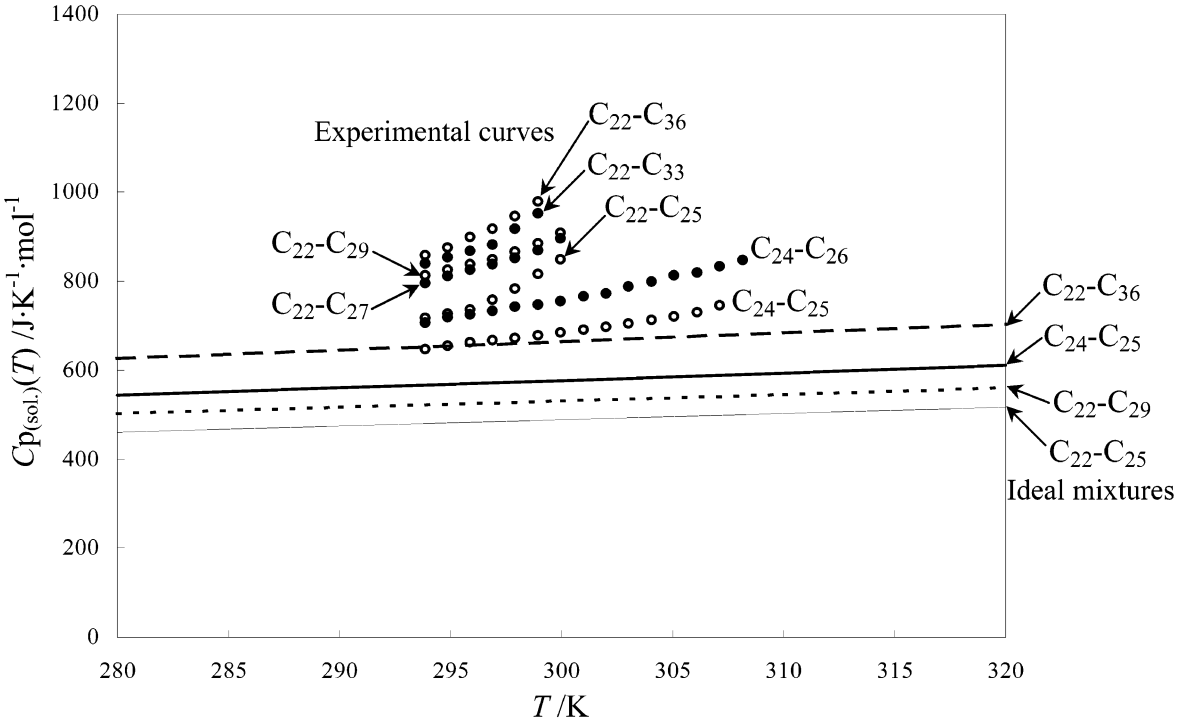

Figure 7. Comparison between the smoothed curves of experimental heat capacities, in the ordered solid phases near the ordered/disordered transition temperatures, of group 1 and 2 mixtures versus temperature. Variations in equivalent ideal mixtures (−), situated in the linear part of the function, stemming from Eintein solid's model ($C_p(T)$, eq 1).

ment of energy, called the "energy of formation of the solid phase". By deduction, the greater the chain lengths' disparity, the higher the energy, the more significant the molecular disorder, and the greater the deviation in relation to ideality. However, this correlation between the amplitude of the deviation in relation to the ideality and the C_n distribution width is not clearly noticeable, although we note a behavior very close to ideality for the binary mixture C_{24}−C_{25} ($\bar{n}$ = 24.5) (Figure 6).

(d) Heat Capacities in the Ordered Solid Phase. The experimental heat capacity variations of the ordered phase and those calculated for the equivalent ideal mixtures ($\overline{C_p} = \Sigma_{i=1}^{N} x_i C_{p_i}$) are reported in Figure 7 as a function of the temperature. The C_{p_i} heat capacities of pure C_n's are calculated by the predictive equation stemming from the Einstein solid model, established in a previous paper,[1] as follows:

$$C_p(T) = 3NR\left(\frac{\theta}{T}\right)^2 \frac{\exp^{(\theta/T)}}{(\exp^{(\theta/T)} - 1)^2} + cT + dT^2 \qquad (1)$$

with $C_p(T)$/J·K^{-1}·mol^{-1}, the heat capacity of the C_n in the

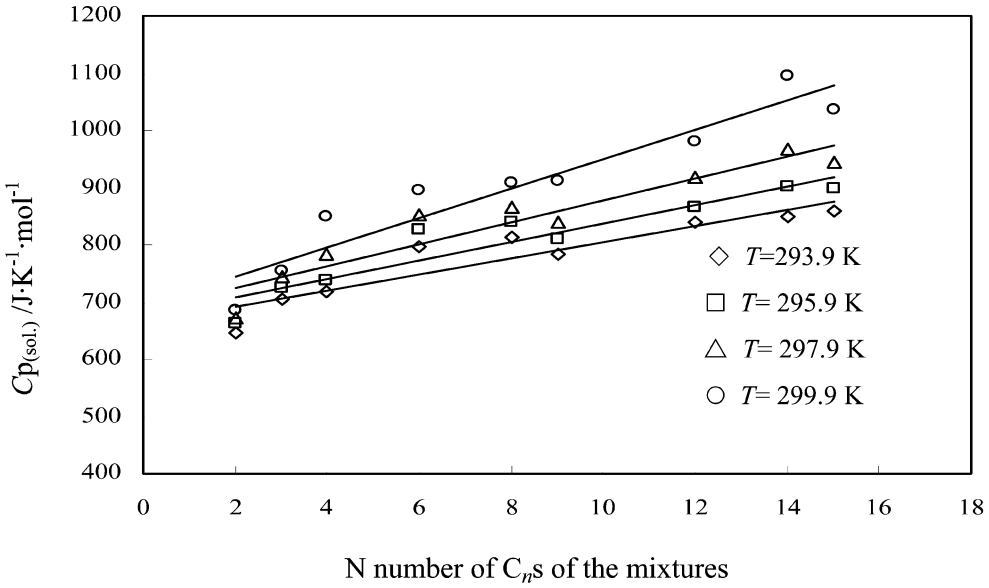

Figure 8. Isothermal evolutions of the heat capacity in the ordered solid phase as a function of the N number of C_n's of the samples.

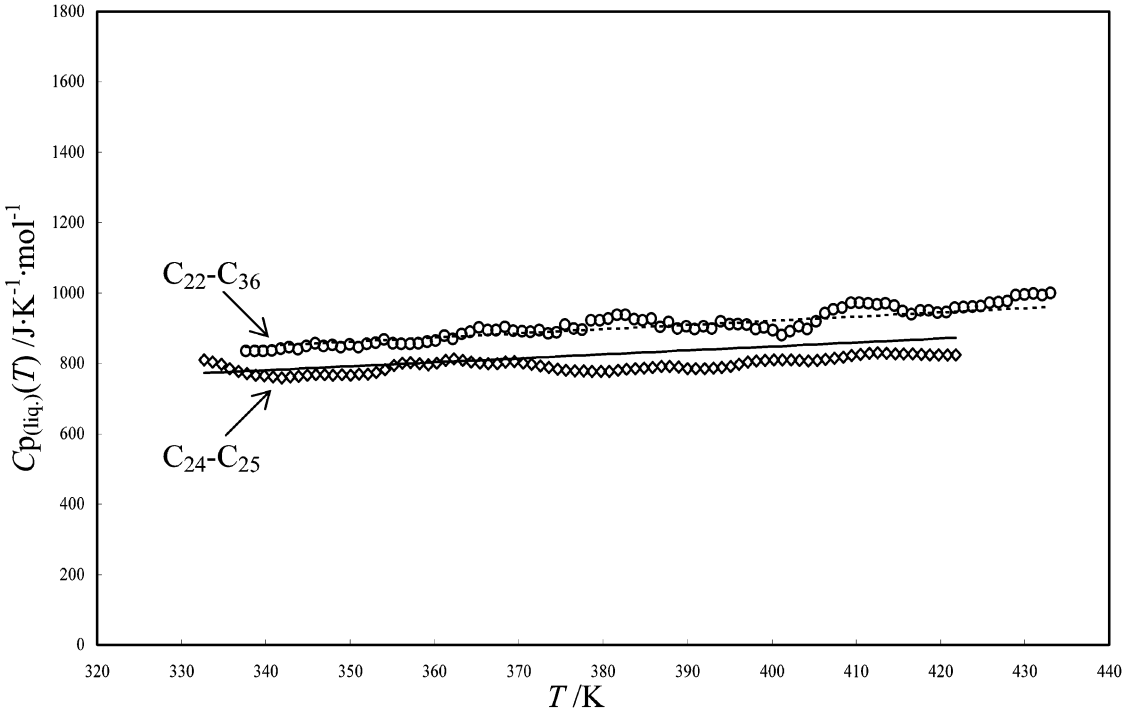

Figure 9. Comparison between the smoothed curves of the experimental heat capacities, in the liquid phase, of group 1 and 2 samples versus temperature and those of equivalent ideal mixtures calculated by $C_{p(\mathrm{liq})}$ (eq 2).

solid ordered phase at constant pressure ($P = P_0 = 1$ atm); T/K, the considered temperature; R/J·K^{-1}·mol^{-1}= 8.314, the perfect gas constant; N, the number of oscillators per C_n molecule (each C_n molecule behaves like a monatomic solid of N atoms having $3N$ independent harmonic vibrations); θ, the Einstein temperature characteristic of the oscillation frequency of the harmonic vibrations of the atoms; and c/K^{-2} and d /K^{-3}, the coefficients of the quadratic part introduced to take into account the skeletal vibrational contribution.

The four parameters N, θ, c, and d are all functions of the n number[1] of carbon atoms of the C_n chain.

The comparison of the experimental and ideal C_p values (Figure 7) and the experimental C_p variations as a function of N, represented by the isotherm curves of Figure 8, involve the following comments:

(i) Because of the mixture effect, the experimental heat capacity values are always higher than the equivalent ideal mixture values: the arrangement of molecules of different lengths in a single multi-C_n solid phase is more disordered than the equivalent assemblage of the "almost perfect" crystals of pure C_n's. Greater disorder generates weaker molecular interactions and, thus, a higher amplitude of oscillatory movements, which leads to higher heat capacity values,

(ii) The gap between experimental and ideal values (Figures 7) and the C_p experimental values (Figures 8) increase in relation to the following: The N number of C_n's of the x_n distribution because increasing the N number of different molecules induces greater disorder in the molecular layers. The temperature that exponentially increases the conformational defects[4] in the carbon chains in the

course of heating (not taken into account by the Einstein model[1]), particularly near the solid−solid transition temperature.

(e) Heat Capacities in the Liquid Phase. The experimental $C_{p(liq)}$ heat capacity variations in the liquid phase, as a function of the temperature, are reported in Figure 9 for two samples and are compared with the variations calculated for their ideal mixture, equivalent to a pure C_n with the number of carbon atoms equal to the $\bar{n}$ real average number of carbon atoms of the mixture distribution. The ideal heat capacity values were calculated by the relation derived from the group contribution method and established for pure C_n's in a previous paper[1]:

$$C_{p(liq)}/J\cdot K^{-1}\cdot mol^{-1} = (0.0343\bar{n} + 0.2855)T + 24.587\bar{n} - 203.370 \quad (2)$$

$$\bar{n} = \sum_{n_{min}}^{n_{max}} x_n n$$

$\bar{n}$: real mean number of carbon atoms of mixtures

All of the liquid mixtures studied present the same behavior, whatever the distribution width and the mean composition. As for the two cases of Figure 9, the heat capacities increase linearly with respect to the temperature, and good agreement is observed between experimental and ideal values. The multiparaffinic liquid mixtures do not show any excess heat capacity,[17,29−33] related to two possibilities: a nil excess enthalpy or an excess enthalpy independent of the temperature.

Measurements of the mixing enthalpy of two multi-C_n liquid phases, carried out by mixing calorimetry,[17] and previous calorimetric experiments of paraffinic mixture dissolving in hydrocarbon liquid phases[29−33] confirm the athermal behavior of multi-C_n synthetic mixtures in the liquid state: the experimental specific enthalpy of mixing of two paraffinic complex liquids[17,29−33] is lower than 1 $J\cdot g^{-1}$.

This behavior can be generalized to all the multi-C_n liquid mixtures, whatever their composition and the N number of C_n's: their heat capacity can estimated by the $Cp_{(liq)}$ previous eq 2.

Synthetic and Commercial Multi-C_n Mixtures with C_n Mole Fraction Distributions of the Normal Logarithmic Type

Sample Characterization. The industrial and commercial multi-C_n samples show x_n mole fraction continuous distributions of consecutive C_n's of the normal logarithmic type[5−7,9,10] (Figure 1d). According to Pauly et al.[34] and Dauphin et al.,[35] the complex liquid mixtures, whose x_n distributions are the exponential decreasing type (Figure 1a) as observed in petroleum cuts, form solid deposits with x_n distributions of the normal logarithmic type. Calorimetric analyses are also required to determine the thermodynamic properties of these complex mixtures, which are defined as follows:

(i) Four commercial mixtures purchased from Prolabo, called in its commercial catalog paraffins 52−54 °C, 54−56 °C, 58−60 °C ,and 60−62 °C; they are respectively denoted P1, P2, P3, and P4. They are mainly composed of consecutive C_n's, from C_{20}, with $23 \leq N \leq 33$. The other nonlinear hydrocarbons are branched alkanes or naphtens (Table 4). Their structural and thermodynamic states were described in the literature.[4−8]

Table 4. Compositions in C_n's of the Mixtures with x_n Distributions of the Normal Logarithmic Type[a]

	S1	S2	P1	P2	P3	P4
C_{20}			0.07	0.05	0.02	0.04
C_{21}			0.77	0.45	0.06	0.18
C_{22}	2.2	1.9	4.63	2.89	0.44	0.68
C_{23}	4.5	2.8	12.82	8.00	1.81	2.08
C_{24}	7.9	3.9	20.09	13.10	5.08	4.25
C_{25}	11.7	5.2	18.32	14.35	9.19	6.59
C_{26}	14.9	6.6	14.64	15.46	14.46	8.48
C_{27}	16.2	8	9.40	13.26	15.63	10.62
C_{28}	14.9	9.1	6.76	11.44	15.81	11.76
C_{29}	11.7	9.8	4.85	8.85	14.00	11.72
C_{30}	7.9	10.1	3.51	6.24	11.37	10.38
C_{31}	4.5	9.8	2.28	3.45	7.14	8.81
C_{32}	2.2	9.1	1.02	1.56	3.28	6.70
C_{33}	0.9	8	0.39	0.56	1.10	5.07
C_{34}	0.3	6.6	0.18	0.21	0.38	3.57
C_{35}	0.1	5.2	0.09	0.08	0.13	2.59
C_{36}	0.02	3.9	0.06	0.03	0.05	1.83
C_{37}			0.04	0.02	0.02	1.42
C_{38}			0.03	0.01	0.01	1.04
C_{39}			0.02	0.01	0.01	0.64
C_{40}			0.01	0.01	0.00	0.49
C_{41}			0.01			0.32
C_{42}			0.01			0.25
C_{43}						0.16
C_{44}						0.11
C_{45}						0.07
C_{46}						0.06
C_{47}						0.03
C_{48}						0.02
C_{49}						0.02
C_{50}						0.02
C_{51}						0.01
C_{52}						0.01
$\bar{n}_c$	27.1	29.7	25.6	26.4	27.8	29.4
$\bar{M}$	381.5	417.5	328.6	372.0	390.6	413.2
%C_n's	100	100	93.69	86.92	86.43	76.72

[a] S1 and S2 multiparaffinic synthetic and P1, P2, P3, and P4 commercial mixtures.

(ii) Two synthetic mixtures (denoted S1 and S2), obtained by melting 15 pure C_n's ranging from C_{22} to C_{36} (Table 4, Figure 1b and c):

−S1: variance of 2.50 and shifting of the center of the Gaussian law of 1.5 carbon atoms toward light C_n's;

−S2: variance of 4.35 and shifting of 1.5 carbon atoms toward heavy C_n's.

The structural analyses carried out by X-ray diffraction at ambient temperature (T = 294.15 K)[4−8] reveal that all of these commercial and synthetic mixtures form a single solid solution, isostructural to the β' ordered intermediate phase of binary and ternary C_n alloys.[14−16]

Results and Discussion. The experimental order/disorder transition and melting onset and end temperatures, the transition enthalpies, and the (ΔH/kJ·mol^{-1} and Δh/J·g^{-1}) total enthalpy variations are given in Table 5 with the compositional characteristics of each mixture. The experimental enthalpy ($H_{T_o}^{T}$/kJ·mol^{-1} or h/J·g^{-1}; T_o = 293.4 K) increments with respect to the temperature are listed for each sample in Supporting Information. Figure 10 shows the specific enthalpy increment curve as a function of the increasing temperature obtained for P4. With increasing temperature, all of the mixtures undergo order/disorder and disorder/disorder solid/solid transitions identical to those of the odd-numbered C_n's, with the successive appearance of the high-temperature disordered rotator orthorhombic β-RI($Fmmm$) and rhomboedric α-RII-($R\bar{3}m$) structures.[4,7]

Phase-Transformation Temperatures and Enthalpies. The variations in the experimental transition tem-

Table 5. Experimental Thermodynamic Properties of S1 and S2 Synthetic Mixtures and of P1, P2, P3, and P4 Commercial Waxes[a]

					melting			order/disorder			total	
mixtures	$\bar{n}$	$\bar{M}$ /g·mol^{-1}	%C$_n$'s	N of C$_n$'s	ΔT_{fus} /K	$\Delta^d_{fus}H$ /kJ·mol^{-1}	$\Delta^d_{fus}h$ /J·g^{-1}	ΔT_{o-d} /K	ΔH_{o-d} /kJ·mol^{-1}	Δh_{o-d} /J·g^{-1}	$\Delta H^{T_{fus}}_{T_{o-d}}$ /kJ·mol^{-1}	$\Delta h^{T_{fus}}_{T_{o-d}}$ /J·g^{-1}
S1	27.1	381.5	100	15	327.7−331.4	62.6	164.0	312.5−315.8	19.8	52.0	93.7	245.7
S2	29.7	417.5	100	15	?−339.7			324.9− ?			102.1	244.4
P1	25.6	328.6	93.7	23	323.2−326.3		146.1	304.0−308.7		46.4		233.0
P2	26.4	372.0	86.9	21	324.8−328.7		144.3	307.2−313.5		37.9		221.8
P3	27.8	390.6	86.4	21	328.2−332.1		150.3	311.1−318.6		44.1		227.0
P4	29.4	413.2	76.7	33	327.7−334.6		147.4	311.2−319.4		39.7		229.1

[a] $\Delta T_{fus}(\pm 0.5)$/K, temperature range of melting; $\Delta^d_{fus}H$/kJ·mol^{-1} and J·g^{-1} (% diff = 3%), enthalpy of melting; $\Delta T_{o-d}(\pm 0.5)$/K, temperature range of order/disorder transition; ΔH_{o-d}/J·mol^{-1} and J·g^{-1} (% diff = 3%), enthalpy of order/disorder transition; $\Delta H^{T_{fus}}_{T_{o-d}}$/kJ·mol^{-1} and J·g^{-1} (% diff = 3%); enthalpy variation from T_{o-d} to $T_{fus(end)}$.

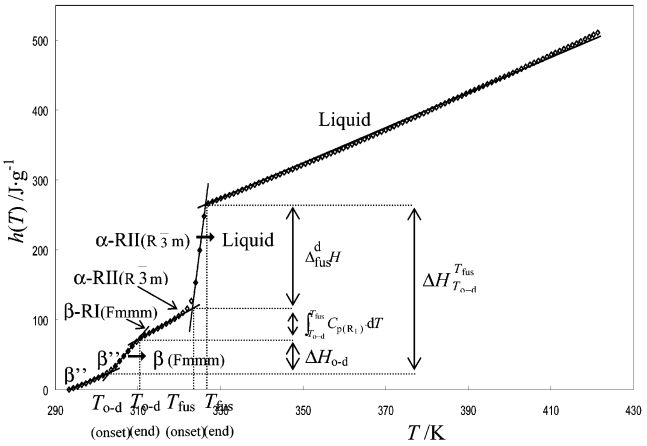

Figure 10. Specific enthalpy curve ($h^T_{T_o}$/kJ·g^{-1}; T_o = 293.4 K) for the P1 real wax from the β'' ordered phase up to the liquid phase above the melting point.

peratures and specific enthalpies are reported in Figure 11 as functions of the $\bar{n}$ real average number of carbon atoms of the single solid phase of mixtures, and they are compared with the $\bar{T}$ average melting temperatures ($\bar{T}_{fus} = \Sigma_{i=1}^{N} x_i T_{fus\ i}$) and transformation specific enthalpies[1] of equivalent ideal solid solutions ($\Delta\bar{h} = \Sigma_{i=1}^{N} x_i \Delta h_i$; $\Delta h^{T_{fus}}_{T_{o-d}}$/J·g^{-1} = 269; $\Delta^d_{fus}h$/J·g^{-1}= 165; Δh_{o-d} /J·g^{-1} = 72)[1]. To highlight the influence of the shape of the x_n distribution on the thermodynamic behavior of the synthetic paraffinic mixtures, the phase-transformation temperatures and enthalpies of the two-phase sample C_{22}−C_{36} of group 2, composed of same consecutive pure C$_n$'s ranging from C_{22} to C_{36} (Figure 1a) and denoted S3, are reported in Figure 11:

(i) The transformation temperatures of S1 are closer to the calculated average temperatures than those of S3. For sample S2, the order/disorder transition and melting temperatures are very close, and an accurate separation of the two transformations is not possible. Only the value of the $\Delta h^{T_{fus}}_{T_{o-d}}$ total enthalpy appears in Table 5. The order/disorder transition onset temperature of S2 is higher than those of the S1 and S3 because its composition is richer in heavy C$_n$'s.

(ii) The gap between measured and calculated temperatures is constant for P1, P2, and P3, but it considerably increases for P4 (Figure 11), which presents a higher percentage of nonlinear hydrocarbons and an N higher C$_n$ number (Table 4). However, these gaps are slightly greater than those of S1 and S2 but slightly lower than that of S3.

The phase-transformation specific enthalpies of single-phase samples S1 and S2 show behavior closer to ideality than those of two-phase sample S3 (Figure 11). P1, P2, P3, P4, and S3 reveal similar deviations between the experimental enthalpy values and those of equivalent ideal mixtures (Figure 11). The presence of other hydrocarbons involves in P1, P2, P3, and P4 deviations in relation to the ideality identical to that observed in two-phase sample S3.

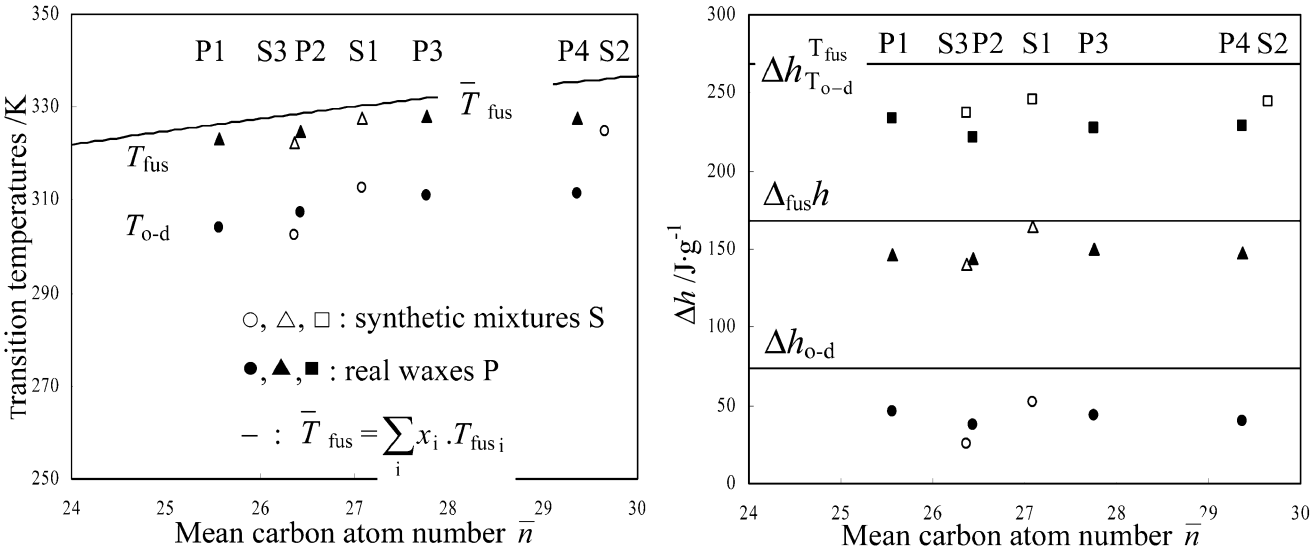

Figure 11. Evolutions of the experimental temperatures and specific enthalpies of phase transformations of S1, S2, S3, P1, P2, P3, and P4 samples versus their $\bar{n}$ real mean number of carbon atoms compared to the corresponding values of equivalent ideal mixtures[1] (−): $\Delta h^{T_{fus}}_{T_{o-d}}$/J·g^{-1} = 269; $\Delta^d_{fus}h$/J·g^{-1}= 165; Δh_{o-d}/J·g^{-1} = 72.

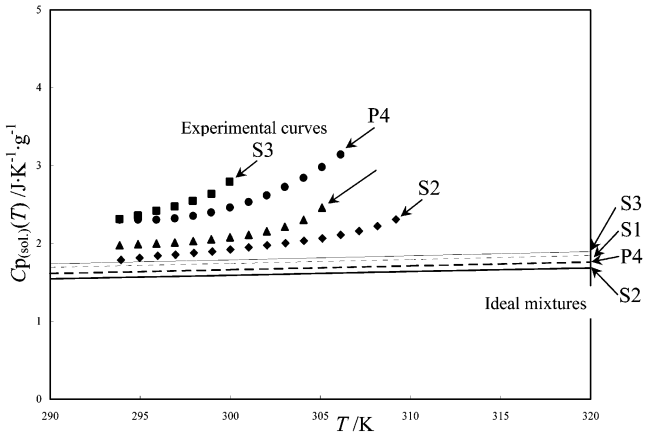

Figure 12. Comparison between the smoothed curves of the experimental heat capacities, in the ordered solid phases, of S1, S2, S3, and P4 versus temperature and the values of equivalent ideal mixtures (−), situated in the linear part of the function, stemming from thte Eintein solid model ($C_p(T)$, eq 1).

These results highlight the fact that the disorder is higher in synthetic mixtures with a x_n distribution of the exponential decreasing type (Figure 1a) than in samples with a x_n distribution of the normal logarithmic type composed of the same C_n's (Figure 1b and c). In the mixtures with x_n distributions of the normal logarithmic type, the value of the $\bar{n}$ average number of carbon atoms of the single solid phase is situated at the center of gravity of the Gaussian curve (Figure 1b−d) near the majority of C_n's, which impose single-crystalline organization and a single c parameter corresponding to a molecular layer thickness close to the mean length of their chain, on the lighter and heavier minority C_n's. In the case of x_n distributions of the exponential decreasing type, the value of $\bar{n}$, the average number of carbon atoms of the mixtures, is situated near C_n's that are not the majority (Figure 1a). For C_n numbers of $N \geq 12$, single-crystalline organization can be imposed neither by these minority C_n's nor by the C_n's, the lightest of which here are the majority but are too short; this state leads to a higher conformational disorder in these single- or polyphase mixtures.

For the commercial mixtures, the higher internal disorder in relation to that of S1 and S2 is generated by a higher N number of C_n's and the ratio of the other hydrocarbons (Table 4).

Whatever the characteristics of the distribution, the synthetic and real mixtures in the solid state present a difference between the thermodynamic experimental results and the ideal values. This gap indicates the enthalpy of formation of the solid solution, which always positive.

Heat Capacity Variations as a Function of the Temperature

Heat Capacities in the Ordered Solid Phase. Figure 12 depictes the experimental specific heat capacity variations of P4, S1, S2, and S3 and those of ideal mixture values ($\overline{C_p} = \Sigma_{i=1}^{N} x_i C_{p_i}$) as a function of temperature in the low-temperature ordered phases: C_{p_i} of pure C_n's calculated according to eq 1.

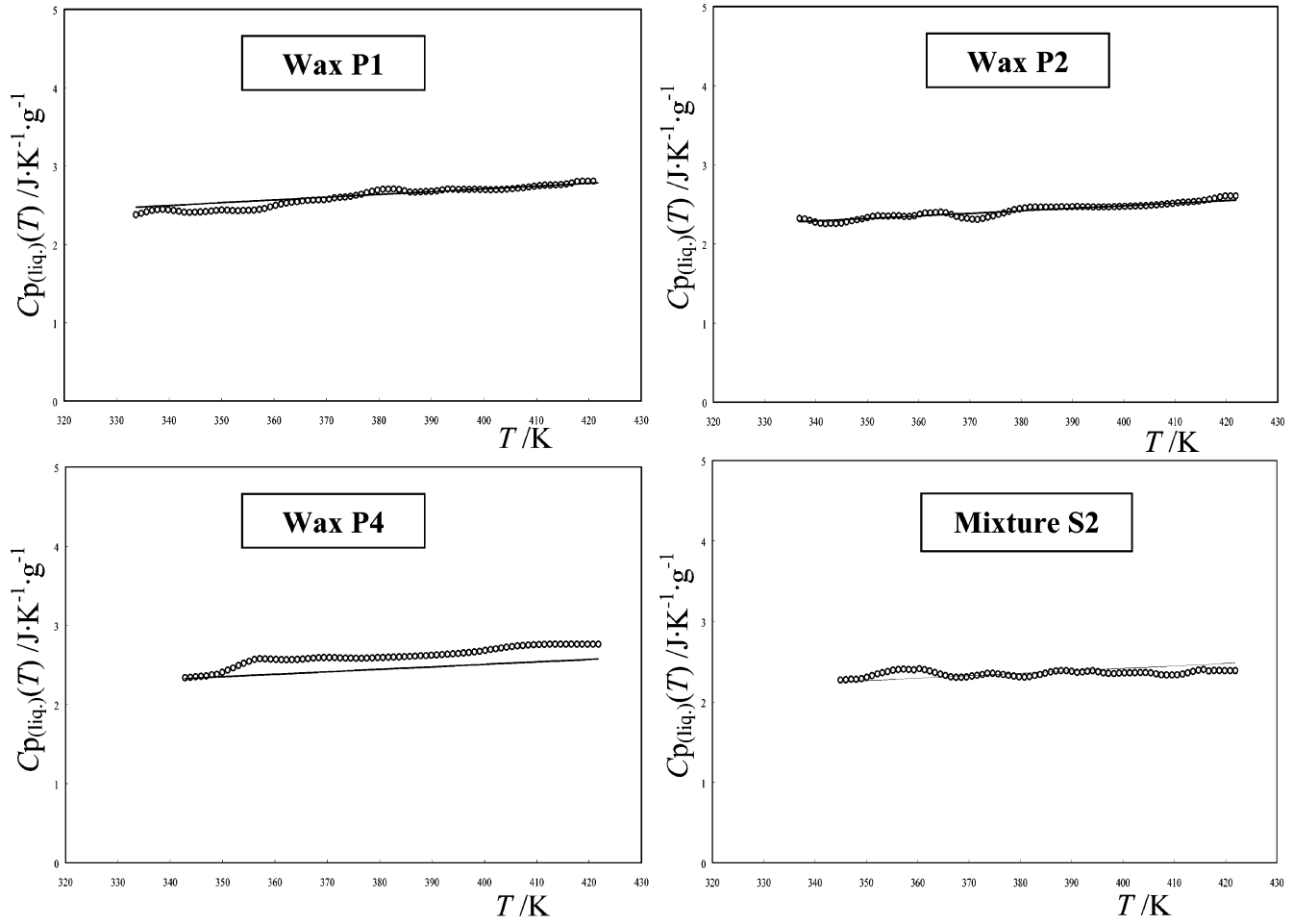

Figure 13. Comparison between the smoothed variations of the experimental heat capacities, in the liquid phase, of P1, P2, P4, and S2 versus temperature and those of equivalent ideal mixtures (−), calculated by $C_{p(liq)}$ (eq 2).

The analysis of the results leads to the following observations:

(i) The experimental heat capacity values are always higher than those calculated for an ideal mixture (because of the mixture effect) and increase gradually at the approach of the order/disorder transition temperatures.

(ii) The heat capacities of S1 and S2 are much lower than those of S3. In S1 and S2 the Gaussian law of x_n distributions leads to a single ordered phase with stronger intermolecular interactions,

(iii) P1, P2, P3, and P4, whose heat capacity values are similar, show significant gaps between ideal and experimental results; they can be imposed by the ratio of other hydrocarbons and/or the width of the distribution. These deviations in relation to the ideality in the ordered solid phase are close to those observed for S3.

Heat Capacities in the Liquid Phase. Figure 13 compares the variations in the S2, P1, P2, and P4 experimental specific heat capacities to the values (eq 2) of C_n equivalent ideal mixtures,[1] in relation to temperature in the liquid phase.

The experimental heat capacities in the liquid phase of all of the mixtures vary linearly as a function of the temperature, and they are in good agreement with ideal liquid mixture values (Figure 13). This result is valid for all of the samples, except for the wax P4 that reveals higher heat capacities than those of the equivalent ideal liquid. This gap could be explained by a higher ratio of the other hydrocarbons and of heavier C_n's from C_{40} to C_{60}: these heavy C_n's bring about a more significant internal disorder associated with mechanisms of folding, deformation, and tangling of carbon chains, which increase the heat capacity values.[2] According to Van Miltenburg[36] and Atkinson,[37] in a liquid-phase temperature range from the melting point up to 30−40 K, the heat capacities of heavy C_n do not follow a linear variation law in relation to the temperature. This peculiar behavior corresponds to the supplementary enthalpy consumption needed to break the residual order in the liquid phase and to obtain molecules completely desoriented above the melting point.

Conclusions

Thermodynamic studies were carried out on 18 multi-C_n synthetic and 4 real mixtures by differential scanning calorimetry with discontinuous or continuous temperature programming. The ($H^T_{T_o}$/kJ·mol^{-1}; $h^T_{T_o}$/J·g^{-1}; T_o = 293.4 K) enthalpy increment measurements of all of the samples are described as a function of the temperature in Supporting Information.

From the structural[4−16] and thermodynamic[1−3,17,19,20] literature results, these studies highlight the following observations:

(i) S1 and S2 synthetic and P1, P2, P3, and P4 real mixtures with normal logarithmic type x_n distributions of an N number of consecutive C_n's ($15 \le N \le 33$) are in a crystalline single-phase solid state.

(ii) The synthetic mixtures with exponential decreasing type x_n distributions are in a single-phase state if $N \le 11$ or in a two-phase ($12 \le N \le 16$) or three-phase ($17 \le N \le 21$) state.

The melting onset temperatures, which depend on solid themodynamic state,

(i) vary linearly as a function of $\bar{n}$, the average number of carbon atoms ($22 \le \bar{n} \le 25$), of the multi-C_n solid solution in single-phase systems, with the $\bar{T}_{fus}$ average melting temperatures ($\bar{T}_{fus} = \Sigma_{i=1}^{N} x_i T_{fus\ i}$), calculated from the pure C_n values. The influence of nonlinear hydrocarbons, which, according to the literature,[5,6,10] form an amorphous solid in the real petroleum mixtures, is weak with regard to the behavior of transformation temperatures of P1, P2, and P3, except for P4 where their ratio is higher;

(ii) depend on $\bar{n}_c$ the mean number of carbon atoms of the lightest phase for the transformation onset temperatures and of the heaviest phase for the transformation end temperatures in the polyphase systems.

The comparison between experimental thermodynamic properties and corresponding values calculated for C_n equivalent ideal mixtures shows a deviation in relation to the ideality in the ordered solid state of all the mixtures:

(i) For the enthalpies (Figures 6 and 11), this deviation is higher for the single-phase synthetic mixtures with exponential decreasing type x_n distributions and is much greater for the polyphase synthetic mixtures and in the (multi-C_n crystalline single-phase + amorphous solid) real mixtures than for the single-phase synthetic systems with normal logarithmic type x_n distributions.

(ii) For the heat capacities, this deviation increases in relation to the increase in the N number of C_n's and the complexity in the mixtures and of the temperature (Figures 7 and 12); in all cases, this induces an increase in disorder. For the mixtures with the same C_n's, the deviation in relation to ideality is higher for the synthetic mixtures, with exponential decreasing type x_n distributions, and for the real mixtures than for the single-phase synthetic mixtures, whose x_n distributions are of the normal logarithmic type. For these latter mixtures, the crystalline organization, imposed by the majority C_n's, is more coherent, and the molecular interactions are greater.

In the liquid state, whatever the N number of C_n's and their molecular length differences, the enthalpy of C_n mixing is athermal[17,29−33] ($\Delta H^{exc}_{liq} = 0$), and the behavior of all of the liquid multi-C_n mixtures is ideal, except for P4 whose nonlinear hydrocarbon ratio is higher.

In the solid state, these results highlight a gap in relation to the ideality due to a formation energy of one or several multi-C_n ordered solid solutions that always is positive. The modeling of the mixtures' thermodynamic behavior needs the determination of the excess properties of the mixtures, calculated from the experimental thermodynamic values in this article, from their mixing enthalpies[17] and from the pure C_n thermodynamic data.[1−3,38] This research is the subject of another study.[17]

Supporting Information Available:

Enthalpy increment versus temperature for C_n mixtures, S1 and S2 mixtures, and P1−P4 waxes. This material is available free of charge via the Internet at http://pubs.acs.org.

Literature Cited

(1) Briard, A. J.; Bouroukba, M.; Petitjean, D.; Dirand, M. Models for Estimation of Pure *n*-Alkanes' Thermodynamic Properties as a Function of Carbon Chain Length. *J. Chem. Eng. Data*, **2003**, *48*, 1508−1516.

(2) Briard, A. J.; Bouroukba, M.; Petitjean, D.; Hubert, N.; Dirand, M. Experimental Enthalpy Increments from the Solid Phases to the Liquid Phase of Homologous *n*-Alkane Series (C_{18} to C_{38} and C_{41}, C_{44}, C_{46}, C_{50}, C_{60}). *J. Chem. Eng. Data* **2003**, *48*, 497−513.

(3) Dirand, M.; Bouroukba, M.; Briard, A. J.; Chevallier, V.; Petitjean, D.; Corriou, J. P. Temperatures and Enthalpies of Solid + Solid and Solid + Liquid Transitions of *n*-Alkanes. *J. Chem. Thermodyn.* **2002**, *34*, 1255−1277.

(4) Dirand, M.; Bouroukba, M.; Chevallier, V.; Petitjean, D. Normal Alkanes, Multialkane Synthetic Model Mixtures, and Real Petroleum Waxes: Crystallographic Structures, Thermodynamic Properties, and Crystallization. *J. Chem. Eng. Data* **2002**, *47*, 115−143.

(5) Dirand, M.; Bouroukba, M.; Chevallier, V.; Provost, E.; Petitjean, D. Multicomponent Paraffin Waxes and Petroleum Solid Deposits: Structural and Thermodynamic State. *Fuel* **1998**, *77*, 1253−1260.

(6) Chevallier, V.; Provost, E.; Bourdet, J. B.; Bouroukba, M.; Petitjean, D.; Dirand, M. Mixtures of Numerous Different *n*-Alkanes − I. Structural Studies by X-ray Diffraction at Room Temperature − Correlation between the Crystallographic Long c Parameter and the Average Composition of Multi-Alkane Phases. *Polymer* **1999**, *40*, 2121−2128.
(7) Chevallier, V.; Petitjean, D.; Bouroukba, M.; Dirand, M. Mixtures of Numerous Different *n*-Alkanes − II. Studies by X-ray Diffraction and Differential Thermal Analyses with Increasing Temperature. *Polymer* **1999**, *40*, 2129−2137.
(8) Chevallier, V.; Briard, A. J.; Petitjean, D.; Hubert, N.; Bouroukba, M.; Dirand, M. Influence of the Distribution General Shape of *n*-Alkane Mole Concentrations on the Structural State of Multi-Alkane Mixtures. *Mol. Cryst. Liq. Cryst.* **2000**, *350*, 273−291.
(9) Craig, S. R.; Hastie, G. P.; Roberts, K. J.; Gerson, A. R.; Sherwood, J. N.; Tack, R. D. Investigation into the Structures of Binary-, Tertiary- and Quinternary Mixtures of *n*-Alkanes and Real Diesel Waxes Using High-Resolution Synchrotron X-ray Powder Diffraction. *J. Mater. Chem.* **1998**, *4*, 859−869.
(10) Retief, J. J.; Le Roux, J. H. Crystallographic Investigation of a Paraffinic Fischer−Tropsch Wax in Relation to a Theory of Wax Structure and Behaviour. *S. Afr. J. Sci.* **1983**, *79*, 234−239.
(11) McCrorie, J. W. Some Physical Properties of Dental Modelling Waxes and of Their Main Constituents. *J. Oral Rehabil.* **1974**, *1*, 29−45.
(12) Chevallier, V.; Petitjean, D.; Ruffier-Meray, V.; Dirand, M. Correlations between the Crystalline Long c-Parameter and the Number of Carbon Atoms of Pure *n*-Alkanes. *Polymer* **1999**, *40*, 5953−5956.
(13) Craig, S. C.; Hastie, G. P.; Roberts, K. J.; Sherwood, J. N. Investigation into the Structures of Some Normal Alkanes within the Homologous Series $C_{13}H_{28}$ to $C_{60}H_{122}$ Using High-Resolution Synchrotron X-ray Powder Diffraction. *J. Mater. Chem.* **1994**, *4*, 977−981.
(14) Dirand, M.; Achour, Z.; Jouti, B.; Sabour, A. Binary Mixtures of *n*-Alkanes. Phase Diagram Generalization: Intermediate Solid Solutions, Rotator Phases. *Mol. Cryst. Liq. Cryst.* **1996**, *275*, 293−304.
(15) Nouar, H.; Bouroukba, M.; Petitjean, D.; Dirand, M. Ternary Phase Diagram *n*-Docosane:*n*-Tricosane:*n*-Tetracosane Molecular Alloys at 293 K. *Mol. Cryst. Liq. Cryst.* **1998**, *309*, 273−282.
(16) Nouar, H.; Petitjean, D.; Bouroukba, M.; Dirand, M. Isothermal Sections of Ternary Mixtures: *n*-Docosane + *n*-Tricosane + *n*-Tetracosane. *Mol. Cryst. Liq. Cryst.* **1999**, *326*, 381−394.
(17) Briard, A. J.; Bouroukba, M.; Dirand, M. Estimation of the Enthalpy of Multialkane Synthetic Mixtures: Measurement by Mixing Calorimetry and Modeling by the Uniquac Model. *J. Chem. Eng. Data* **2004**, *49*, 899−906.
(18) Hanrot, F.; Ablitzer, D.; Houzelot, J. L.; Dirand, M. Experimental Measurement of the True Specific Heat of Coal and Semi-Coke during Carbinization. *Fuel* **1994**, *73*, 305−309.
(19) Achour, Z.; Sabour, A.; Dirand, M.; Hoch, M. Thermodynamic Properties of the *n*-Alkanes $C_{19}H_{40}$ to $C_{26}H_{54}$ and Their Binary Phase Diagrams. *J. Therm. Anal.* **1998**, *51*, 477−488.
(20) Jouti, B.; Bouroukba, M.; Balesdent, D.; Dirand, M. Enthalpy Variation of the Nine Solids Phases of the Binary Molecular Alloys (*n*-Tricosane:*n*-Pentacosane) vs Temperature. *J. Therm. Anal.* **1998**, *54*, 785−802.
(21) Calvet, E.; Prat H. E. In *Microcalorimétrie: Applications Physico-Chimiques et Biologiques*; Masson: Paris, 1956.
(22) Messerly, J. F.; Guthrie, G. B.; Todd, S. S.; Finke, H. L. Low-Temperature Thermal Data for *n*-Pentane, *n*-Heptadecane, and *n*-Octadecane: Revised Thermodynamic Functions for the *n*-Alkanes C_5−C_{18}. *J. Chem. Eng. Data* **1967**, *3*, 338−346.
(23) Andon, R. J. L.; Martin, J. F. Thermodynamic Properties of Hexacosane. *J. Chem. Therm.* **1976**, *8*, 1159−1166.
(24) Chevallier, V.; Bouroukba, M.; Petitjean, B. D.; Dupuis, P.; Dirand, M. Temperatures and Enthalpies of Solid−Solid and Melting Transitions of the Odd-Numbered *n*-Alkanes C_{21}, C_{23}, C_{25}, C_{27}, and C_{29}. *J. Chem. Eng. Data* **2001**, *46*, 1114−1122.
(25) Sabour, A.; Bourdet, J. B.; Bouroukba, M., Dirand, M. Binary Phase Diagram of the Alkane Mixtures *n*-C_{23}:*n*-C_{24}: Modifications. *Thermochim. Acta* **1995**, *249*, 269−283.
(26) Jouti, B.; Provost, E.; Petitjean, D.; Bouroukba, M.; Dirand, M. Phase Diagram of *n*-Tricosane and *n*-Pentacosane Mixtures. *Mol. Cryst. Liq. Cryst.* **1996**, *287*, 275−283.
(27) Jouti, B.; Provost, E.; Petitjean, D.; Bouroukba, M.; Dirand, M. Phase Diagram of *n*-Heneicosane and *n*-Tricosane Molecular Alloys. *J. Mol. Struct.* **1996**, *382*, 49−56.
(28) Nouar, H.; Bouroukba, M.; Petitjean, D.; Dirand, M. Binary Phase Diagram of the System *n*-Docosane−*n*-Tricosane. *J. Mol. Struct.* **1998**, *443*, 197−204.
(29) Ghogomu, P. M.; Dellacherie, J.; Balesdent, D. Solubility of nOrmal Paraffin Hydrocarbons (C_{20} to C_{24}) and Some of Their Binary Mixtures (C_{22} + C_{24}) and (C_{23} + C_{24}) in Ethylbenzene. *J. Chem. Thermodyn.* **1989**, *21*, 925−934.
(30) Ghogomu, P. M.; Bouroukba, M.; Dellacherie, J.; Balesdent, D.; Dirand, M. On the Ideality of Liquid Mixtures of Long-Chain *n*-Alkanes. *Thermochim. Acta* **1997**, *306*, 69−71.
(31) Ghogomu, P. M.; Bouroukba, M., Dellacherie, J.; Balesdent, D.; Dirand, M. Calorimetric Measurement of Mole Excess Enthalpies of Dilute Solutions of Ethylbenzene + Higher *n*-Alkanes. *Thermochim. Acta* **1997**, *302*, 159−164.
(32) Ghogomu, P. M.; Bouroukba, M.; Dellacherie, J.; Balesdent, D.; Dirand, M. Excess Thermodynamic Properties of Some Binary Solutions of Ethylbenzene + *n*-Alkanes. *Thermochim. Acta* **1997**, *302*, 151−158.
(33) Provost, E.; Chevallier, V.; Bouroukba, M.; Dirand, M.; Ruffier-Meray, V.; Behar, E. Experimental Determination and Representation of Binary and Ternary Diagrams of *n*-Hexacosane, *n*-Octacosane and *n*-Heptane. *La Revue de l' I. F. P.* **1998**, *53*, 27−33.
(34) Pauly, J.; Dauphin, C.; Daridon, J. L. Liquid−Solid Equilibria in a Decane + Multi-Paraffins System. *Fluid Phase Equilib.* **1998**, *149*, 191−207.
(35) Dauphin, C.; Daridon, J. L.; Coutinho, J. A. P.; Baylère, J.; Potin-Gautier, M. Wax Content Measurements in Partially Frozen Paraffinic Systems. *Fluid Phase Equilib.* **1999**, *161*, 135−151.
(36) Van Miltenburg, J. C. Fitting the Heat Capacity of Liquid *n*-Alkanes: New Measurements of *n*-Heptadecane and *n*-Octadecane. *Thermochim. Acta* **2000**, *343*, 57−62.
(37) Atkinson, C. M. L.; Larkin, J. A.; Richardson, M. J. Enthalpy Changes in Molten *n*-Alkanes and Polyethylene. *J. Chem. Thermodyn.* **1969**, *1*, 435−440.
(38) Briard, A. J.; Bouroukba, M.; Petitjean, D.; Dirand, M. Variation of Dissolution Enthalpies of Pure *n*-Alkanes in Heptane as a Function of Carbon Chain Length. *J. Chem. Eng. Data* **2003**, *48*, 1574−1577.

Received for review October 17, 2003. Accepted June 7, 2004.

JE0302405